

The density of states method at non-zero chemical potential

Zoltan Fodor^{a,b,c}, Sandor D. Katz^b and Christian Schmidt^{a,d}

^a*Department of Physics, University of Wuppertal, Gauss 20, D-42119, Germany*

^b*Institute for Theoretical Physics, Eötvös University, Pázmány 1, H-1117 Budapest, Hungary*

^c*Department of Physics, University of California at San Diego, 9500 Gilman Drive, La Jolla, CA 92093-0319, USA*

^d*Department of Physics, Brookhaven National Laboratory, Upton, 11973, NY, USA*

ABSTRACT: We study the QCD phase diagram by first principle lattice calculations at so far unreachable high densities. For this purpose we employ the density of states method. Unimproved staggered fermions, which describe four quark flavors in the continuum are used in this analysis. Though the method is quite expensive, small lattices show an indication for a triple-point connecting three different phases on the phase diagram.

KEYWORDS: Thermal Field Theory, Lattice QCD.

Contents

1. Introduction	1
2. Formulation of the method	2
2.1 Simulations with constrained Plaquette	3
2.2 Generating Configurations with measure $ \det M(\mu) $	4
3. Simulation details and the strength of the sign problem	4
4. The Plaquette expectation value and the phase diagram	7
5. The quark number density	10
6. Conclusions	11

1. Introduction

To clarify the phase diagram of QCD and thus the nature of matter under extreme conditions is one of the most interesting and fundamental tasks of high energy physics. The experimental setup of the running Relativistic Heavy Ion Collider (RHIC) at the Brookhaven National Laboratory, as well as the forthcoming Large Hadron Collider (LHC) at CERN, aim on the creation of hot quark matter, the quark gluon plasma. Future experiments like the Compressed Baryonic Matter (CBM) experiment at the Facility for Antiproton and Ion Research (FAIR), attempt to explore the phase diagram in the region of high temperatures and intermediate densities. On the theoretical side various color-superconducting phases have been proposed in the region of very high densities but low temperatures, which may be relevant to the physics of neutron star interiors. For a review see for example [1].

Lattice QCD has been shown to provide important and reliable information from first principles on QCD at zero density. However, lattice QCD at finite densities has been harmed by the complex action problem ever since its inception. At non-zero chemical potentials ($\mu > 0$) the determinant of the fermion matrix ($\det M$) becomes complex. Standard Monte Carlo techniques using importance sampling are thus no longer applicable when calculating observables in the grand canonical ensemble according to the partition function

$$Z_{GC}(\mu) = \int \mathcal{D}U \det M[U](\mu) \exp\{-S_G[U]\}. \quad (1.1)$$

Note that Z_{GC} is real. The origin of the sign problem are the fluctuations of the complex phase θ , defined by $\det M \equiv |\det M| \exp\{i\theta\}$. In case those fluctuations ($\sqrt{\langle(\theta - \langle\theta\rangle)^2}\rangle$) become considerably larger than $\pi/2$ [2], the problem becomes serious. For a detailed

discussion of the phase of the fermion determinant see also [3]. Recently many different methods have been developed to circumvent the complex action problem for $\mu/T \lesssim 1$ [4, 5]. For a recent overview see also [6]. With all these methods the transition line of the QCD phase transition was mapped in the (T, μ) -plane. The results coincide for small chemical potentials and the same choice of parameters.

The goal of this paper is to employ the density of states method at non-zero chemical potential to extend the accessible region of the QCD phase diagram to lower temperatures and higher densities. The paper is organized as follows: In Section 2 we introduce our method and in Section 3 we give the details of our simulation parameters. Readers who are not interested in the details of our method or the simulation parameters may start at Section 4, where we will discuss results on the phase diagram. Results for the quark number density will be given in Section 5. Finally we will conclude in Section 6.

2. Formulation of the method

A very general formulation of the DOS method is the following: One special parameter (ϕ) is held fixed. The expectation value of a thermodynamic observable (O), according to the usual grand canonical partition function (1.1), can be recovered by the integral over ϕ ,

$$\langle O \rangle = \int d\phi \langle Of(U) \rangle_\phi \rho(\phi) \bigg/ \int d\phi \langle f(U) \rangle_\phi \rho(\phi) \quad (2.1)$$

where the density of states (ρ) is given by the constrained partition function:

$$\rho(x) \equiv Z_\phi(x) = \int \mathcal{D}U g(U) \delta(\phi - x). \quad (2.2)$$

With $\langle \rangle_\phi$ we denote the expectation value with respect to the constrained partition function. In addition, the product of the weight functions f, g has to give the correct measure of Z_{GC} : $fg = \det M \exp\{-S_G\}$. This idea of reordering the partition functions was used in many different cases [7, 8, 9]. The advantages of this additional integration becomes clear, when choosing $\phi = P$ and $g(U) = 1$. Here P denotes the plaquette expectation value. In this case $\rho(\phi)$ is independent of all simulation parameters. Once $\rho(\phi)$, as well as the correlation between ϕ and the observable O is known, O can be calculated as a continuous function of the lattice coupling β . If one has stored all eigenvalues of the fermion matrix for all configurations, the observable can also be calculated as a function of quark mass (m) and number of flavors [8] (N_f).

In this work we chose

$$\phi = P \quad \text{and} \quad g = |\det M| \exp\{-S_G\}, \quad f = \exp\{i\theta\}. \quad (2.3)$$

In other words we constrain the plaquette and perform simulations with measure g . In practice, we replace the delta function in Eq. (2.2) by a sharply peaked potential [9]. The constrained partition function for fixed values of the plaquette expectation value can then be written as

$$\rho(x) \approx \int \mathcal{D}U g(U) \exp\{-V(x)\}, \quad (2.4)$$

where $V(x)$ is a Gaussian potential with

$$V(x) = \frac{1}{2}\gamma(x - P)^2. \quad (2.5)$$

We obtain the density of states ($\rho(x)$) by the fluctuations of the actual plaquette P around the constraint value x . The fluctuation dissipation theorem gives

$$-\frac{d}{dx} \ln \rho(x) = \langle \gamma(x - P) \rangle_x. \quad (2.6)$$

Before performing the integrals in Eq. (2.1) we carry out a calculation based on an ensemble generated at (μ_0, β_0) :

$$\langle Of(U) \rangle_x(\mu, \beta) = \langle Of(U)R(\mu, \mu_0, \beta, \beta_0) \rangle_x / \langle R(\mu, \mu_0, \beta, \beta_0) \rangle_x, \quad (2.7)$$

$$\langle f(U) \rangle_x(\mu, \beta) = \langle f(U)R(\mu, \mu_0, \beta, \beta_0) \rangle_x / \langle R(\mu, \mu_0, \beta, \beta_0) \rangle_x, \quad (2.8)$$

$$\frac{d}{dx} \ln \rho(x, \mu, \beta) = \langle (x - P)R(\mu, \mu_0, \beta, \beta_0) \rangle_x. \quad (2.9)$$

Here R is given by the ratio of the measure g at the point (μ, β) and at the simulation point (μ_0, β_0) ,

$$R(\mu, \mu_0, \beta, \beta_0) = g(\mu, \beta)/g(\mu_0, \beta_0) = \frac{|\det(\mu)|}{|\det(\mu_0)|} \exp\{S_G(\beta) - S_G(\beta_0)\}. \quad (2.10)$$

Having calculated the expressions (2.7)-(2.9), we are able to extrapolate the expectation value of the observable (2.1) to any point (μ, β) in a small region around the simulation point (μ_0, β_0) . For any evaluation of $\langle O \rangle(\mu, \beta)$, we numerically perform the integrals in Eq. (2.1). We also combine the data from several simulation points as described by Eqs. (2.7)-(2.9).

2.1 Simulations with constrained Plaquette

The quantity we want to constrain is the real part of the plaquette $P_{\mu\nu}(y)$ averaged over lattice points (y) and directions (μ, ν)

$$P = \sum_y \sum_{1 \leq \mu < \nu \leq 4} \frac{1}{3} \text{ReTr} P_{\mu\nu}(y). \quad (2.11)$$

Since the plaquette is also the main part of the gauge action,

$$S_G = -\beta \sum_x \sum_{1 \leq \mu < \nu \leq 4} \left\{ \frac{1}{3} \text{ReTr} P_{\mu\nu}(x) - 1 \right\}, \quad (2.12)$$

the additional potential V , which constraints the plaquette around a given value, can be easily introduced in the hybrid Monte Carlo update procedure of the hybrid-R algorithm [10]. To do so we modify the force in the molecular dynamical evolution of the gauge field by a factor $(1 + \gamma(x - P)/\beta)$. This requires the measurement of the plaquette in each molecular dynamical step.

2.2 Generating Configurations with measure $|\det M(\mu)|$

For the generation of Configurations with measure g , according to Eq. (2.3) we use the method of Ref. [11]. Since at finite iso-spin chemical potential the fermion determinant is real, our fermion matrix in flavor space is given by

$$M = \begin{pmatrix} M_{KS}(\mu) & \lambda\gamma_5 \\ -\lambda\gamma_5 & M_{KS}(-\mu) \end{pmatrix}. \quad (2.13)$$

Here each component represents a usual staggered fermion field χ with four flavors in the continuum limit. The diagonal elements are thus the usual staggered fermion matrices, in the upper left corner with chemical potential μ and in the lower right corner with chemical potential $-\mu$. The off-diagonal elements are iso-spin symmetry breaking terms, proportional to the small parameter λ , which are necessary in order to see spontaneous symmetry breaking on a finite lattice. The fermion matrix (2.13) will thus represent eight continuum flavor. Note that the γ_5 matrices corresponds in the staggered case to a multiplication of the phase $\epsilon(x) = -1^{x_1+x_2+x_3+x_4}$.

In order to simulate this system, we use the HMC in complete analogy to the even-odd ordering of the $\mu = 0$ case. This means that we generate Gaussian noise (R) for both components of $(R_1, R_2) = M(\chi_1, \chi_2)$, but keep only the upper component (χ_1) after the inversion. This way we still describe eight flavors with the block-diagonal positive definite matrix $M^\dagger M$ which we use for the evolution of the gauge field. In the molecular dynamical integration of the equations of motion, we perform the usual square-root trick to reduce the number of flavors to four. In the limit of $\lambda \rightarrow 0$ it is however correct to take the square-root and will not introduce any approximations or locality problems, since our basic building block is the four flavor staggered fermion matrix which comes out with a power of one. A further reduction of n_f to two or one, by using a fractional power of the staggered fermion matrix, introduces additional difficulties that are still under debate [12]. It is known [13] that using the square (or forth) root of the staggered matrix at $\mu > 0$ could lead to phase ambiguities.

3. Simulation details and the strength of the sign problem

Simulations have been performed with staggered fermions and $N_f = 4$. We chose 9 different points in the $(\beta, a\mu)$ -plane for the 4^4 lattice and 8 points for the 6^4 lattice. On each of these points we did simulations with 20-40 constrained plaquette values, all with quark mass $am = 0.05$. Further simulations have been done with $(\beta, a\mu) = (5.1, 0.3)$ on the $6^3 \times 8$ lattice for $am = 0.05$ and $am = 0.03$. The simulation points and statistics are summarized in Table 1. For each point $(\beta, a\mu)$ we have chosen several plaquette values in the range where the density of states (ρ) is large. In addition we measure all eigenvalues of the reduced fermion matrix. Here “reduced” means that the μ dependence was reduced by Gauss elimination to the first and last time slice. This procedure was described in detail in Ref. [4]. Having stored the eigenvalues, we are able to evaluate the fermionic determinant (absolute value and phase) as a function μ , as well as all their derivatives.

N_s	N_t	β	am	$a\mu$	P	λ	#
4	4	4.850	0.05	0.30	2.26-3.59	0.01, 0.02	$2 \times 44 \times 4000$
4	4	4.850	0.05	0.35	2.26-3.59	0.01	$1 \times 44 \times 4000$
4	4	4.850	0.05	0.40	2.26-3.59	0.01, 0.02	$2 \times 44 \times 4000$
4	4	4.850	0.05	0.45	2.26-3.59	0.01	$1 \times 44 \times 4000$
4	4	4.850	0.05	0.50	2.26-3.59	0.01	$1 \times 44 \times 4000$
4	4	4.950	0.05	0.40	2.26-2.59	0.01	$1 \times 44 \times 4000$
4	4	4.925	0.05	0.40	2.26-2.59	0.01	$1 \times 44 \times 4000$
4	4	4.900	0.05	0.40	2.26-2.59	0.01	$1 \times 44 \times 4000$
4	4	4.875	0.05	0.40	2.26-2.59	0.01	$1 \times 44 \times 4000$
6	6	5.10	0.05	0.30	2.78-2.98	0.01	$1 \times 16 \times 5715$
6	6	5.10	0.05	0.35	2.75-2.94	0.01	$1 \times 16 \times 8987$
6	6	5.10	0.05	0.40	2.72-2.91	0.01	$1 \times 16 \times 6800$
6	6	5.10	0.05	0.45	2.70-2.89	0.01	$1 \times 16 \times 2303$
6	6	5.18	0.05	0.35	2.70-3.23	0.01	$1 \times 44 \times 3995$
6	6	5.16	0.05	0.35	2.70-3.27	0.01	$1 \times 32 \times 4393$
6	6	5.14	0.05	0.35	2.70-3.23	0.01	$1 \times 32 \times 5915$
6	6	5.12	0.05	0.35	2.70-3.05	0.01	$1 \times 32 \times 6960$
6	8	5.10	0.05	0.30	2.70-3.16	0.01	$1 \times 39 \times 2355$
6	8	5.10	0.03	0.30	2.70-3.14	0.006	$1 \times 32 \times 1360$

Table 1: Simulation parameter and statistics. The number of trajectories is given in the last column, here the first factor is due to the number of the lambda parameters and the second factor gives the number of plaquette values.

In order to calculate the plaquette expectation value, or its susceptibility, one has to perform the following integrals:

$$\langle P \rangle = \int dx x \rho(x) \langle \cos(\theta) \rangle_x, \quad \langle P^2 \rangle = \int dx x^2 \rho(x) \langle \cos(\theta) \rangle_x. \quad (3.1)$$

Thus the functions $\rho(x)$ and $\langle \cos(\theta) \rangle_x$ have to be known quite precisely. We plot both functions in Figure 1. The transition is signaled in the double peak structure of $\rho(x)$. The phase factor $\langle \cos(\theta) \rangle_x$ suppresses the peak of $\rho(x)$ at smaller plaquette values, which results in a shift of the critical temperature to smaller values, in comparison with the phase quenched theory.

In Figure 2 we show the phase factor for different chemical potentials. With increasing chemical potential the phase factor becomes compatible with zero within errors. In fact, its average value becomes as low as $\cos(\theta) \sim 0.005$. There exists however a small interval around $P \sim 2.85$, where the phase factor remains finite. In this way, the Plaquette expectation values are strongly altered by the phase factor. Figure 2 demonstrates also the advantage of the DOS method over the other approaches of lattice QCD at finite density. Using the DOS method one is able to do simulations directly at those Plaquette values which are relevant at finite density. This results in an even better overlap than that of the multi-parameter re-weighting approach.

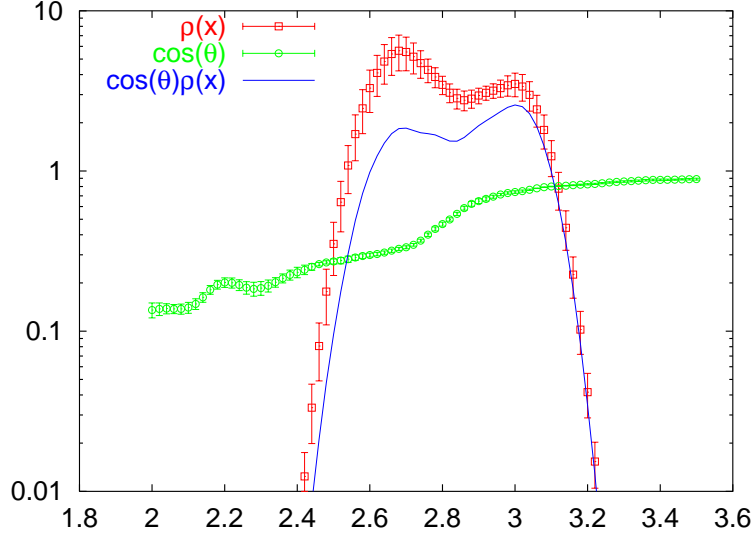


Figure 1: Results for Simulations at $\beta = 4.98$, $\mu = 0.3$, $\lambda = 0.02$, $n_f = 4$, $am = 0.05$, and number of lattice points: 4^4 . Shown are the density of states $\rho(x)$, the phase factor $\langle \cos(\theta) \rangle$, and their product.

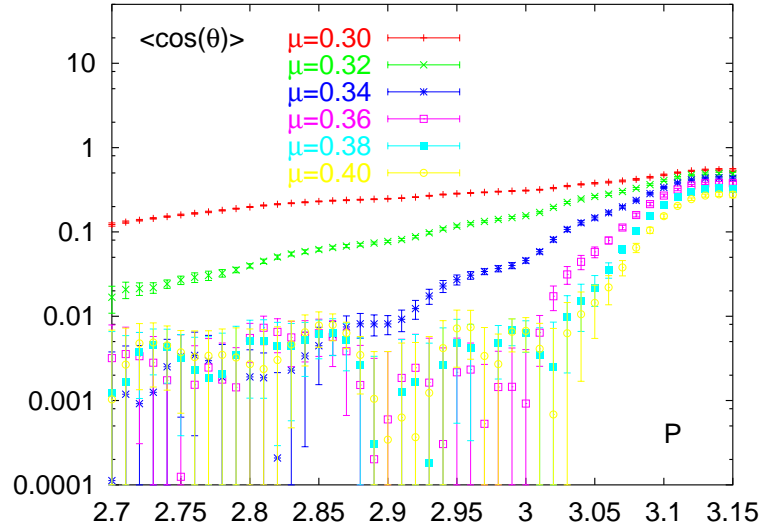


Figure 2: Results for Simulations at $\beta = 5.1$, $\lambda = 0.01$, $n_f = 4$, $am = 0.05$, and number of lattice points: 6^4 . Shown is the suppression from the complex phase of the fermion determinant $\langle \cos(\theta) \rangle$ for different chemical potentials.

In order to be able to transform the lattice units into physical units, we have measured the heavy quark potential on a zero temperature lattice: $10^3 \times 20$. From the potential we determined the Sommer scale r_0 and the string tension σ . In Addition we have measured the pion mass and the nucleon mass. The results are given in Table 2.

β	r_0/a	$a^2\sigma$
4.85	1.436(18)	0.818(5)
4.90	1.537(84)	0.745(12)
5.05	1.711(35)	0.576(9)
5.10	1.876(16)	0.445(7)
5.15	2.208(17)	0.321(3)
5.17	2.411(4)	0.276(1)

β	am_π	am_N
4.85	0.5413(1)	2.40(4)
4.90	0.5447(1)	2.26(3)
5.05	0.5613(2)	2.21(2)
5.10	0.5715(3)	2.17(1)
5.15	0.5892(2)	2.03(1)
5.17	0.5982(1)	1.93(1)

Table 2: Results for the Sommer radius (r_0), string tension (σ), pion mass (m_π) and nucleon mass (m_N) for different β values. The results are for $n_f = 4$ and $am = 0.05$, measured on a $10^3 \times 20$ lattice.

as shown in Figure 4. The extrapolated result $\beta = 4.938(4)$ (including the phase factor) and the result from multi-parameter re-weighting [4] are in very good agreement. The λ dependence is expected to be smaller for larger μ , therefore from now on we only give results for $\lambda/m = 0.2$.

4. The Plaquette expectation value and the phase diagram

Let us now discuss results for the plaquette expectation values from the 6^4 lattice as shown in Figure 5 and Figure 6.

At chemical potentials $\mu \lesssim 0.36$, the plaquette signals the QCD transition through a rapid crossover from a low temperature phase of $\langle P \rangle \sim 2.9$ to a high temperature phase of $\langle P \rangle \sim 3.1$. For $\mu \gtrsim 0.36$ the plaquette expectation value at small temperatures drops to $\langle P \rangle \sim 2.85$. This new low temperature phase of the plaquette at high chemical potentials is caused by the fermion determinant. As one can see in Figure 2 the region around $P \sim 2.85$ is the region which is less suppressed by the phase factor. Another interesting observation is that the critical coupling, which is decreasing in μ for $\mu < 0.36$ starts to increase for $\mu > 0.36$.

The plaquette expectation value thus suggests the existence of three different phases in the (T, μ) -diagram with a triple point, where all those phases coincide. In Figure 7 we show the phase diagram in physical units. The phase boundaries were determined by calculating the peaks in the plaquette susceptibility. The points at $T = 93$ MeV are from calculations

To transform the results from lattice to physical units in practice, the Sommer parameter r_0 was used and has been fitted with a polynomial of the order three, to get the lattice spacing a as a continuous function of β . For r_0 in physical units we have used the MILC result of $r_0 = 0.476(7)(18)$ fm [14].

First of all we check, whether we can reproduce old results with our new method. For this purpose we reproduce one point of the phase transition line which has been calculated by multi-parameter re-weighting from $\mu = 0$ configurations on the 4^4 lattice [4]. Performing the integrations in Eq. (3.1) numerically, we calculate the plaquette expectation value and the plaquette susceptibility $\chi_P \equiv \langle P^2 \rangle - \langle P \rangle^2$. At any fixed λ , we determine the critical coupling by the peak position of the susceptibility as shown in Figure 3. We indeed find that including the phase factor does shift the transition to lower values of the coupling, which also means to lower temperatures. This can be clearly seen in a shift of the peak of the plaquette susceptibility.

Since the λ parameter introduces a systematic error, we have to perform a linear $\lambda \rightarrow 0$ extrapolation

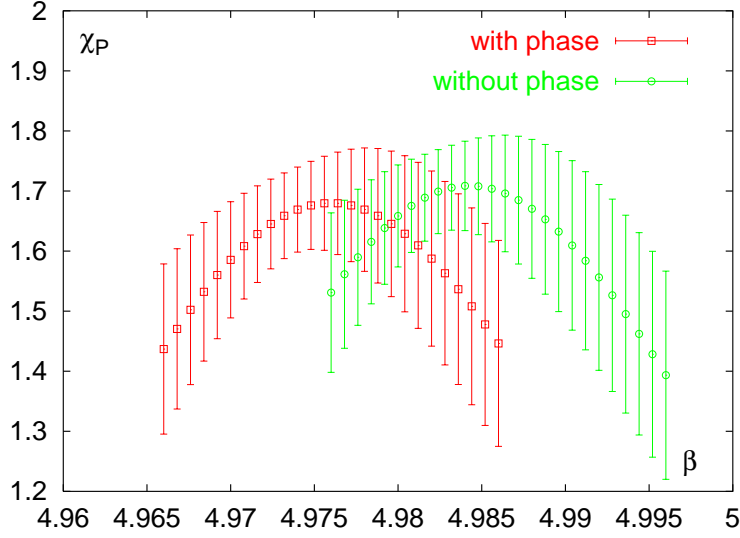


Figure 3: Simulation parameters as in Figure 1. Shown is the plaquette susceptibility as function of the coupling β .

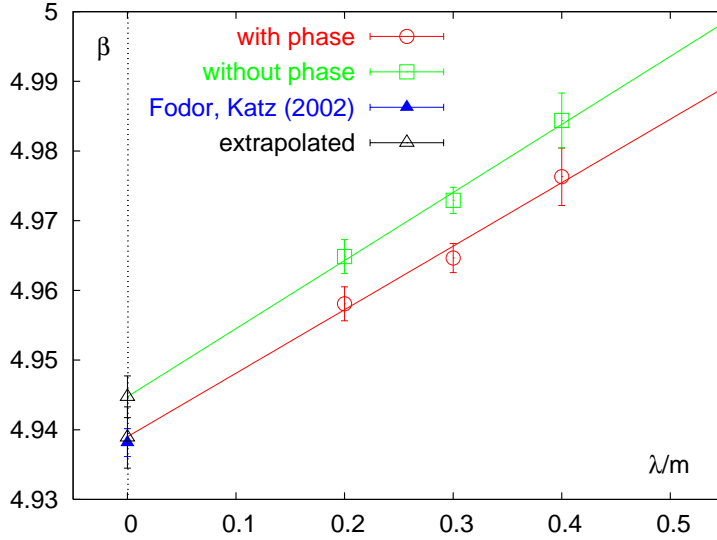


Figure 4: The $\lambda \rightarrow 0$ extrapolation of the critical couplings on the 4^4 lattice at $a\mu = 0.3$.

on $6^3 \times 8$ lattices. Note, that we make no statement about the order of the transition lines. To determine the order of the transition one has to perform a finite-size-scaling analysis which is beyond the scope of this article.

The triple point is located around $\mu_q^{\text{tri}} \approx 300$ MeV, however its temperature (T^{tri}) decreases from $T^{\text{tri}} \approx 148$ MeV on the 4^4 lattice to $T^{\text{tri}} \approx 137$ MeV on the 6^4 lattice. This shift reflects the relatively large cut-off effects one faces, with standard staggered fermions and temporal extents of 4 and 6.

Also shown in Figure 7 are points from simulations with quark mass $am = 0.03$. The

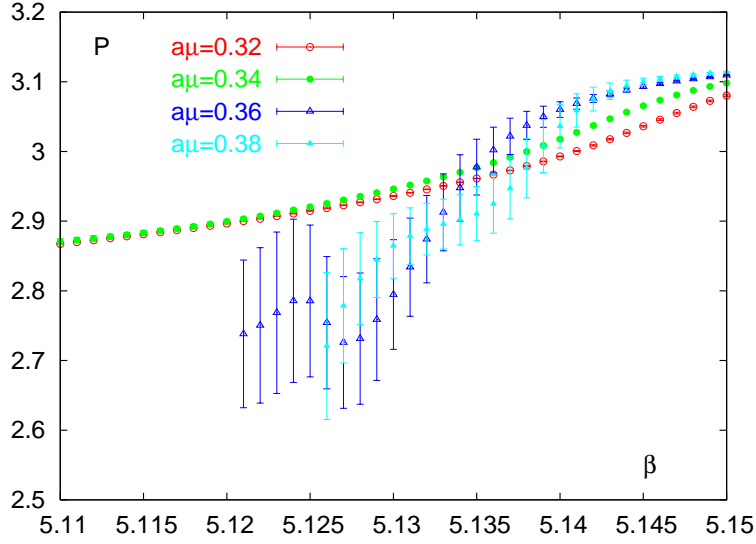


Figure 5: Results for Simulations at $\beta = 5.1$, $\lambda = 0.01$, $n_f = 4$, $am = 0.05$, and number of lattice points: 6^4 . Shown is the Plaquette expectation value as a function of the coupling β for different chemical potentials

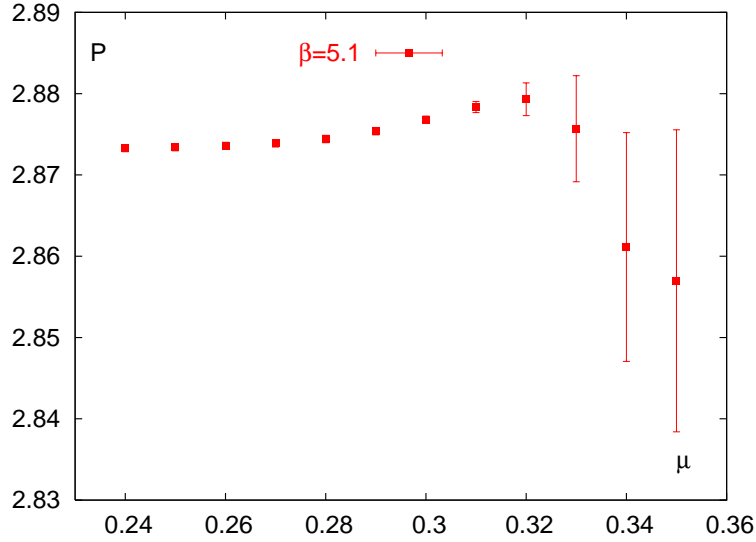


Figure 6: Simulation parameters as in Figure 3. Shown is the plaquette expectation value at fixed coupling, as a function of the chemical potential.

phase boundary at low temperatures turned out to be — within our statistical uncertainties — independent of the the mass. This gives evidence that the transition is associated with the onset of baryonic matter rather than a pion condensate. Going from $am = 0.05$ to $am = 0.03$, the pion mass changes by a factor of $\approx \sqrt{3/5} = 0.77$ whereas the nucleon mass remains approximately constant.

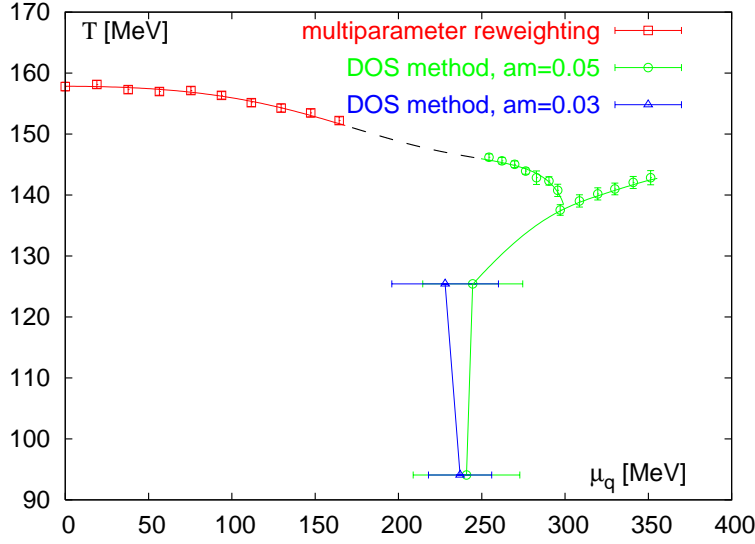


Figure 7: The phase diagram in physical units from $N_t = 6$ and 8 lattices.

5. The quark number density

To reveal the properties of the new phase located in the lower right corner of the phase diagram, we calculated the quark number density, at constant coupling β and at constant temperature respectively. To obtain the density n_q we perform the following integration

$$\left\langle \frac{d \ln \det M}{d(a\mu)} \right\rangle = \int dx \left\langle \frac{d \ln \det M}{d(a\mu)} \cos(\theta) \right\rangle_x \rho(x) \quad (5.1)$$

The thermodynamic quantity n_q are given as usual by

$$n_q = \frac{1}{a^3 N_s^3 N_t} \left\langle \frac{d \ln \det M}{d(a\mu)} \right\rangle \quad (5.2)$$

In Figure 8 we show the baryon number density, which is related to the quark number density by $n_B = n_q/3$. The results are plotted in physical units and correspond to a constant temperature of $T \approx 143$ MeV (4^4 lattice), $T \approx 124$ MeV (6^4 lattice) and $T \approx 93$ MeV ($6^4 \times 8$ lattice). In order to remove the leading order cut-off effect, we have multiplied the data with the factor $c = SB(N_t)/SB$, which is the Stefan-Boltzmann value of a free lattice gas of quarks at a given value of N_t , divided by its continuum Stefan-Boltzmann value. For unimproved staggered fermions this correction factor can be as large as 2 and will not completely remove all the cutoff effects.

At the same value of the chemical potential where we find also a peak in the susceptibility of the plaquette (μ_c), we see a sudden rise in the baryon number density. Thus for $\mu > \mu_c$ we enter a phase of dense matter. The transition occurs at a density of $(2-3) \times n_N$, where n_N denotes nuclear matter density. Above the transition, the density reaches values of $(10-20) \times n_N$. Quite similar results have been obtained recently by simulations in the canonical ensemble [15].

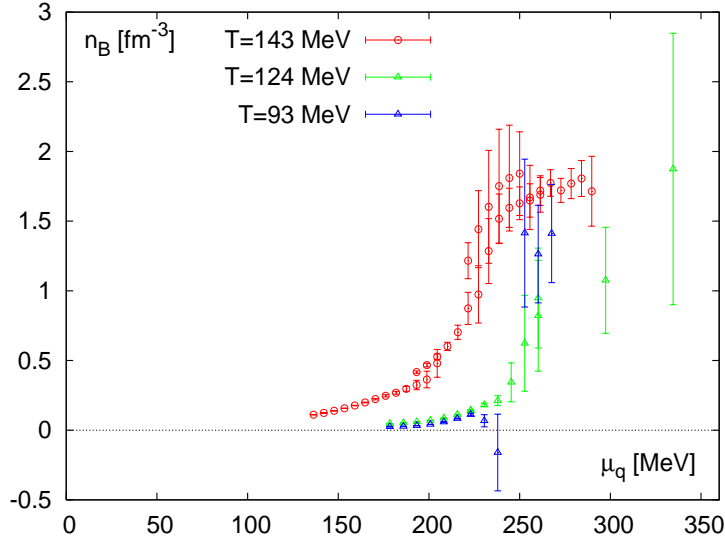


Figure 8: The quark number density at constant temperature $T = 143$ MeV (4^4 lattice), $T = 124$ MeV (6^4 lattice) and $T = 93$ MeV ($6^3 \times 8$ lattice).

6. Conclusions

We have explored the QCD phase diagram by first principle lattice calculations at so far unreachable high densities. In the accessible region of $T \gtrsim 100$ MeV and $\mu_q \lesssim 400$ MeV we have been able to identify three different regions, which seem to be separated by different plaquette expectation values and quark number densities. These regions coincide in a triple-point. The triple-point has been located at $T^{\text{tri}} \lesssim 137$ MeV and $m_q^{\text{tri}} \approx 300$ MeV at finite lattice spacing ($N_t = 6$). We note, that the lowest reachable temperature on $N_t = 6$, is about 60 MeV (setting the scale e.g. by m_ρ). We thus find the triple-point about 80 MeV above the lowest temperature. This is the first numerical evidence from lattice QCD for a third phase (apart from the hadronic phase and the quark gluon plasma) and a triple point in the QCD phase diagram. In the third phase the quark number density reaches values of $(10 - 20) \times n_N$, where n_N denotes normal nuclear matter density.

The new phase is a natural candidate for a color superconducting phase. Recently, by combining experimental results from cold atoms in a trap [16] and some universal arguments, an upper bound for the transition line from the quark gluon plasma phase (QGP) to the superconducting phase (SC) was proposed ($T_c \leq 0.35 E_F$) [17, 18]. To first approximation the Fermi-Energy E_F is given by the chemical potential μ_q . In [18] the triple point was estimated by comparing this upper bound with the experimental freeze-out curve. A temperature of $T^{\text{tri}} \leq 70$ MeV was found. Our value of the triple-point roughly corresponds to $T_c \leq 0.46 E_F$. It is interesting that the two values are close.

At low temperatures we find a phase boundary which is very steep and almost independent of μ_q . Although our lowest temperature is 96 MeV an extrapolation to $T = 0$ seems to be reasonable and would yield a critical chemical potential of $\mu_q(T = 0) \approx 250$ MeV or equivalently $\mu_B/T_c(\mu_B = 0) \approx 4.7$. This number appears to be at the lower edge of the

phenomenological expectation of $\mu_B/T_c(\mu_B = 0) \approx 5 - 10$. Note, that our lattice spacing is close to the strong coupling regime and we should feel the influence of the strong coupling limit. Strong coupling expansion calculations in general yield much lower values of $\mu_B/T_c(\mu_B = 0) \lesssim 1.5$ [19].

For this work the density of state method has been employed, which works well on small lattices up to chemical potentials of $\mu_q/T \lesssim 3$ (other methods [4, 5] worked up to $\mu_q/T \lesssim 1$). The method is however extremely expensive and thus will in the near future not yield results close to the thermodynamic limit or the continuum limit, due to limitations in computer resources.

We have to emphasize once more, that the simulations have been carried out on coarse lattices with an unphysical value of $n_f = 4$ degenerate fermion flavor, and that neither the continuum nor the thermodynamic limit has been taken. Since we used unimproved staggered fermions, the corrections due to a finite lattice spacing are large. We also expect corrections due to the finite size of our volume. The simulations have not been performed with a constant quark mass, but $m_q/T = 0.3$ has been held fixed.

Acknowledgments

CS would like to thank F. Karsch, Ph. de Forcrand and K. Splittorff for helpful discussions and comments. CS has partially been supported by a contract DE-AC02-98CH1-886 with the U.S. Department of Energy. ZF and SK have been supported by OTKA Hungarian Science Grants No. T34980, T37615, M37071, T032501, AT049652 and the German Research Grand (DFG) FO 502/1. The computations were carried out at Eötvös University on the 330 processor PC cluster of the Institute for Theoretical Physics and the 1k node PC cluster ALiCENext at the University of Wuppertal, using a modified version of the publicly available MILC code [20] and a next-neighbor communication architecture [21].

References

- [1] M. G. Alford, *Color superconductivity in ultra-dense quark matter*, *PoS LAT2006* (2006) 001 [[arXiv:hep-lat/0610046](#)]; M. Alford and K. Rajagopal, *Color superconductivity in dense, but not asymptotically dense, quark matter*, [arXiv:hep-ph/0606157](#).
- [2] S. Ejiri, *Remarks on the multi-parameter reweighting method for the study of lattice QCD at non-zero temperature and density*, *Phys. Rev.* **D69** (2004) 094506, [[arXiv:hep-lat/0401012](#)].
- [3] K. Splittorff, *The sign problem in the epsilon-regime of QCD*, *PoS LAT2006* (2006) 023 [[arXiv:hep-lat/0610072](#)]; K. Splittorff and J. J. M. Verbaarschot, *Phase of the fermion determinant at nonzero chemical potential*, [arXiv:hep-lat/0609076](#).
- [4] Z. Fodor and S. D. Katz, *A new method to study lattice QCD at finite temperature and chemical potential*, *Phys. Lett.* **B534** (2002) 87, [[arXiv:hep-lat/0104001](#)].
- [5] Z. Fodor and S. D. Katz, *Lattice determination of the critical point of QCD at finite T and μ* , *JHEP* **0203** (2002) 014, [[arXiv:hep-lat/0106002](#)]. C. R. Allton *et al.*, *The QCD thermal phase transition in the presence of a small chemical potential*, *Phys. Rev.* **D66** (2002) 074507, [[arXiv:hep-lat/0204010](#)]; R. V. Gavai and S. Gupta, *Pressure and non-linear*

- susceptibilities in QCD at finite chemical potentials, *Phys. Rev. D* **68** (2003) 034506, [arXiv:hep-lat/0303013]; P. R. Crompton, *Interpolating the free energy density differences of reweighting methods*, [arXiv:hep-lat/0301001]; M. D'Elia and M. P. Lombardo, *Finite density QCD via imaginary chemical potential*, *Phys. Rev. D* **67** (2003) 014505, [arXiv:hep-lat/0209146]; Ph. de Forcrand and O. Philipsen, *The QCD phase diagram for small densities from imaginary chemical potential*, *Nucl. Phys. B* **642** (2002) 290, [arXiv:hep-lat/0205016]; Ph. de Forcrand and O. Philipsen, *The QCD phase diagram for three degenerate flavors and small baryon density*, *Nucl. Phys. B* **673** (2003) 170, [arXiv:hep-lat/0307020]; V. Azcoiti, G. Di Carlo, A. Galante and V. Laliena, *Phase diagram of QCD with four quark flavors at finite temperature and baryon density*, *Nucl. Phys. B* **723**, (2005) 77, [arXiv:hep-lat/0503010].
- [6] C. Schmidt, *Lattice QCD at finite density*, *PoS LAT2006* (2006) 021 [arXiv:hep-lat/0610116]; O. Philipsen, *The QCD phase diagram at zero and small baryon density*, *PoS LAT2005* (2005) 016, [arXiv:hep-lat/0510077].
- [7] G. Bhanot, K. Bitar, S. Black, P. Carter and R. Salvador, *The Partition Function Of $Z(2)$ And $Z(8)$ Lattice Gauge Theory In Four-Dimensions: A Novel Approach To Simulations Of Lattice Systems*, *Phys. Lett. B* **187** (1987) 381; G. Bhanot, K. Bitar and R. Salvador, *On Solving Four-Dimensional $SU(2)$ Gauge Theory By Numerically Finding Its Partition Function*, *Phys. Lett. B* **188** (1987) 246; M. Karliner, S.R. Sharpe and Y.F. Chang, *Zeroing In On $SU(3)$* , *Nucl. Phys. B* **302** (1988) 204; V. Azcoiti, G. di Carlo and A. F. Grillo, *A New Proposal For Including Dynamical Fermions In Lattice Gauge Theories: The Compact QED Case*, *Phys. Rev. Lett.* **65** (1990) 2239; A. Gocksch, *Simulating Lattice QCD At Finite Density*, *Phys. Rev. Lett.* **61** (1988) 2054.
- [8] X. Q. Luo, *Thermodynamical quantities of lattice full QCD from an efficient method*, *Mod. Phys. Lett. A* **16** (2001) 1615.
- [9] J. Ambjorn, K. N. Anagnostopoulos, J. Nishimura and J. J. M. Verbaarschot, *The factorization method for systems with a complex action: A test in Random Matrix Theory for finite density QCD*, *JHEP* **0210** (2002) 062, [arXiv:hep-lat/0208025].
- [10] S. Gottlieb, W. Liu, D. Toussaint, R. L. Renken and R. L. Sugar, *Hybrid Molecular Dynamics Algorithms For The Numerical Simulation Of Quantum Chromodynamics*, *Phys. Rev. B* **35** (1987) 2531.
- [11] J. B. Kogut and D. K. Sinclair, *Quenched lattice QCD at finite isospin density and related theories*, *Phys. Rev. D* **66** (2002) 014508, [arXiv:hep-lat/0201017];
- [12] S. R. Sharpe, *Rooted staggered fermions: Good, bad or ugly?*, *PoS LAT2006* (2006) 022 [arXiv:hep-lat/0610094].
- [13] B. Svetitsky, Y. Shamir and M. Golterman, *Why (staggered fermions)**(1/4) fail at finite density*, arXiv:hep-lat/0609051; M. Golterman, Y. Shamir and B. Svetitsky, *Breakdown of staggered fermions at nonzero chemical potential*, *Phys. Rev. D* **74** (2006) 071501, [arXiv:arXiv:hep-lat/0602026].
- [14] MILC Collaboration, C. Aubin *et al.*, *Light hadrons with improved staggered quarks: Approaching the continuum limit*, *Phys. Rev. D* **70** (2004) 094505, [arXiv:hep-lat/0402030].
- [15] A. Alexandru, M. Faber, I. Horvath and K. F. Liu, *Lattice QCD at finite density via a new canonical approach*, *Phys. Rev. D* **72** (2005) 114513, [arXiv:hep-lat/0507020]; S. Kratochvila and Ph. de Forcrand, *The canonical approach to finite density QCD*, *PoS LAT2005* (2005) 167, [arXiv:hep-lat/0509143].

- [16] V.S. Stepanyuk, L. Niebergall, W. Hergert, P. Bruno, *Ab initio study of mirages and magnetic interactions in quantum corrals*, [arXiv:cond-mat/0502506](#).
- [17] T. Schafer, *From trapped atoms to liberated quarks*, [arXiv:nucl-th/0606019](#).
- [18] E. V. Shuryak, *Locating strongly coupled color superconductivity using universality and experiments with trapped ultracold atoms*, [arXiv:nucl-th/0606046](#).
- [19] N. Kawamoto, K. Miura, A. Ohnishi and T. Ohnuma, *Phase diagram at finite temperature and quark density in the strong coupling limit of lattice QCD for color SU(3)*, [arXiv:hep-lat/0512023](#) and references therein.
- [20] **MILC** Collaboration, *public lattice gauge theory code*, see <http://physics.indiana.edu/~sg/milc.html>.
- [21] Z. Fodor, S. D. Katz, and G. Papp, *Better than \$1/mflops sustained: A scalable pc-based parallel computer for lattice qcd*, *Comput. Phys. Commun.* **152** (2003) 121–134, [[arXiv:hep-lat/0202030](#)].